Australian Earthquake Engineering Society 2012 Conference, Dec 7-9, Queensland

Keynote Lecture

Size Distribution of Seismic Events in Mines

Aleksander J. Mendecki
Institute of Mine Seismology, Australia
E-mail: Aleksander.Mendecki@IMSeismology.org

Abstract

As for earthquakes, the sizes of seismic events induced by mining are, within a certain range, power law distributed: $N(\geq R) = \alpha R^{-\beta}$, where $N(\geq R)$ is the number of events not smaller than R, as measured by seismic potency P, moment M or radiated energy E, α measures the activity rate and β is the exponent, or the β-value.

We analysed different data sets of seismicity related to underground hard rock mining with differing geological structures, mining layout, extraction ratio, depth and rate of mining. The exponent β correlates positively with the stiffness of the system (the ability to resist seismic deformation with increasing stresses), i.e. the stiffer the system the higher the exponent. As mining progresses and the overall stiffness of the rock mass degrades the parameter α tends to increase and β tends to decrease. At high mining rates we observed a negative correlation between β and the fractal dimension of the hypocentres. The uncertainty or unpredictability of R, as measured by Shannon entropy, increased with decreasing β.

For the three data sets analysed in this paper none of the traditional size distribution parameters, namely: α, β or $P_{max1} = \alpha^{1/\beta}$, managed to rate seismic hazard consistently and reliably. However, all parameters incorporating volume mined, V_m, rated hazard appropriately. Since the rate of rock extraction that drives the seismic rock mass response to mining varies, the most conclusive parameters to quantify seismic hazard are those incorporating volume mined.

In almost all cases the data deviates from the classical power law. At the lower end of the size spectrum the observed deviations are mainly due to contamination of data with blasts or due to bad seismological processing, otherwise there is a remarkable fit down to the lowest observable event. At the high end of the scale deviations are rather the rule than the exception, and they are most frequently convex, but in some cases concave. This has serious implications for seismic hazard assessment. Therefore, we show a relation, based on the upper-truncated power law distribution, to estimate the size of the next record breaking event. This relation is a function of β, which in turn is a function of the volume of rock extracted or to be extracted.

Keywords: mine seismology, seismic hazard, power law, record breaking events.

1 Introduction

In a hard rock mass with random heterogeneities and with some regular geological structures under load there are patches of rock resisting deformation where stresses are increasing, patches of diffusion where stresses are decreasing and there are some passive volumes not influenced by loading. Locally, stress build-up and/or strength degradation may lead to fast relaxation via deformation jumps, or seismic events, that radiate and dissipate energy across the system. Over time, the size distribution of these events will, within a certain range, follow the power law

$$N(\geq R) = \alpha R^{-\beta}, \tag{1}$$

where $N(\geq R)$ is the number of events not smaller than R as measured by seismic potency – the product of an average source displacement and rupture area, $P = \bar{u}A$, seismic moment – the product of rigidity and potency $M = \mu P$ or by the radiated energy E. Parameter α measures the level of seismic activity and β is the exponent. The power law (1) is an example of a fat or heavy tail distribution that for large R falls off more slowly than an exponential and much more slowly than a Gaussian (thin tail), see Figure 1.

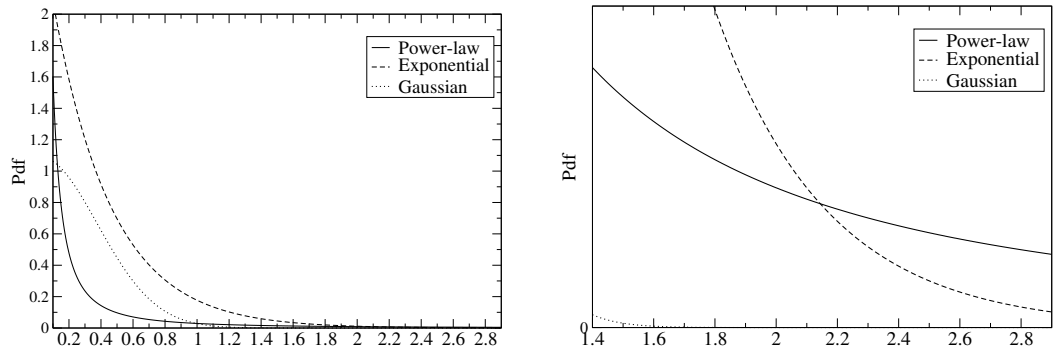

Figure 1: Bodies *(left) and* tails *(right)* of Gaussian (mean $= 10^{-1.9}$ and $s_d = 0.365$), exponential (mean and $s_d = 0.365$), and power law potency distributions with $\beta =$ 0.74, $\log P_{min}$=−1.9, average $\log P$ of the sample $= 0.365$. Parameters are based on data set B, see text.

The probability of a jump in a system described by the Gaussian distribution of sizes is $\Pr(jump) \sim \exp\left(-(jump)^2 / (2s_d^2)\right)$, where s_d is the standard deviation and by the exponential distribution is $\Pr(jump) \sim \exp(-|jump| / s_d)$. The six-sigma event, i.e. $6s_d$ from the mean, has the probability of 10^{-9} of occurring in the case of a Gaussian distribution, whereas it has a 10^{-3} chance in the exponential case – 10^6 times more likely than in the Gaussian case. The power law gives an even higher likelihood of a six-sigma event occurring.

The power law also has the property of scale invariance, i.e the relative change of $N(\geq kR)/N(\geq R) = k^{-\beta}$ is independent of R, therefore it lacks characteristic scale

and puts no prior limit on the maximum event size. Such a scaling can only exist within certain range of sizes, then either the exponent of the distribution or the nature of the distribution need to change to secure a finite energy release. Remarkably, the distribution of sizes of earthquakes for Southern California is observed to be a power law with a constant exponent over more than six orders of magnitude (e.g. *Christensen et al.*, 2002). This scaling is the property of regional dynamics rather than individual faults where it is more complex (e.g. *Wesnousky et al.*, 1983; *Main and Burton*, 1984; *Kijko and Stankiewicz*, 1987; *Wesnousky*, 1994; *Wiemer and Wyss*, 2002). However, some deviations from the power law may lie within the 95% confidence limits of the Poisson process and therefore may not be significant enough to be regarded "characteristic" or "bi-modal" (*Jackson and Kagan*, 2006; *Kagan et al.*, 2012).

In mines the power law scaling has been observed for seismic events as large as m=5.0 (*Mendecki et al.*, 1988) and recently for small fractures with m=−4.0 to −0.3 (*Kwiatek et al.*, 2010), although with varying exponents – seismic events in the low magnitude domain are characterised by higher β.

There is a great deal of speculation on possible mechanism(s) that generate the power law relation. A plausible interpretation is that the crust, or a given seismogenic region, operates in a self organised critical regime or, more precisely, is a part of "slowly driven, interaction dominated threshold systems" (*Jensen*, 1998). In this model (1) the dynamics is dominated by the mutual interaction between different degrees of freedom, (2) the thresholds allow a large number of static metastable configurations and (3) slow loading is important since the strong drive will not allow the system to relax from one metastable configuration to another.

In active mines the extraction of rock is intermittent, and so is the seismic rock mass response to mining. Overall loading is fast and highly variable compared to the tectonic regime. The dynamics here is driven mainly by two competing internal processes, both magnified by the presence of, and occurring mainly close to, excavations and around geological structures.

(1) An excitation due to a sudden loading that moves the system away from its current state and creates an excess level of stress at different locations. It is driven mainly by the transient convergence of excavations in response to rock extraction.

(2) A relaxation, that cascades the system down from its excited non-equilibrium state. It is facilitated by different forms of inelastic deformation – seismic and aseismic. It modifies the stress pattern by reducing its elevated levels and moving it further away from excavations.

Figure 2 shows energy index, EI – a proxy for stress (*van Aswegen and Butler*, 1993) and cumulative seismic displacement, Σu, where $u = 0.00225\sqrt[3]{P}$ (*Somerville et al.*, 1999), plots for a non-productive Sunday and a productive Wednesday. The EI of an event is the ratio of its radiated seismic energy E, to the average energy $\bar{E}(P)$ radiated by events of the same seismic potency P taken from an orthogonal regression line, $\log \bar{E} = d \log P + c$, fitted to data recorded in the area of interest, $EI = E/\bar{E}\,(P)$. For $d = 1.0$, which is not always the case, the energy index is proportional to apparent stress, $EI = 10^{-c}E/P = 10^{-c}\sigma_A$. The higher the energy index, or the apparent stress

for similar potency events, the higher the stress at the source of the event at the time of its occurrence (*Mendecki*, 1993 Figure 1.1; *Mendecki*, 1997, page 189). There is very little activity on Sunday, EI and Σu are both flat. On Wednesday, however, the excitation phase can clearly be seen starting immediately after blasting. The small event of m=0.8 induced, or triggered, by production blasts most likely prolonged the excitation phase.

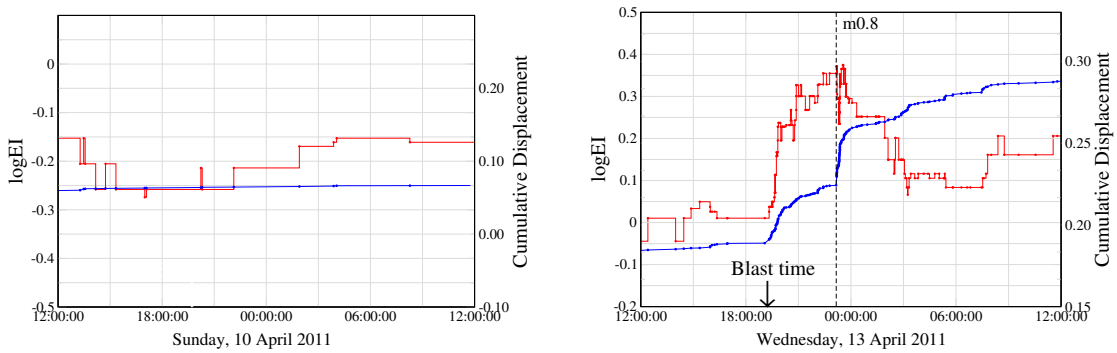

Figure 2: Energy index shown in red and cumulative seismic displacement $u = 0.00225P^{1/3}$ [m], in blue, on time plots during Sunday with no production blasting *(left)* and during Wednesday with excitation phases associated with sudden loading after production blasts *(right)*.

2 Size Distribution Characteristics

Inter-event volume mined. One of the important parameters derived from the size distribution statistics is the mean recurrence time $\bar{t}$ of seismic events above certain size, say seismic potency, $\bar{t}\,(\geq P) = \Delta t/N\,(\geq P)$, where $N\,(\geq P)$ is the number of events above the size P selected from the volume of rock ΔV over the time period Δt. The use of recurrence time is appropriate when driving forces are relatively constant. Since in mines loading is highly variable it is more useful to quote an average inter-event volume mined to generate a seismic event not smaller that a certain size, $\bar{V}_m\,(\geq P) = V_m/N\,(\geq P)$ (*Mendecki and Lötter*, 2011). The $N\,(\geq P)$ is most frequently described by the open-ended relation (OE), see Equation (1) or from the upper-truncated power law (UT) (*Page*, 1968; *Cornell and Vanmarcke*, 1969; *Cosentino et al.*, 1977).

Open-ended power law. Taking the logarithm of Equation (1) and replacing R with P gives $\log N\,(\geq P) = \log\alpha - \beta\log P$, which is the familiar Gutenberg-Richter form $\log N\,(\geq m) = a - bm$, where $a = \log\alpha$, $b = \beta$ and magnitude $m = \log P$. The OE relation allows infinite potency, but *the one largest event* – referred to here as the P_{max1}, is derived from $\alpha P_{max1}^{-\beta} = 1$, that gives $P_{max1} = \alpha^{1/\beta}$ or $\log P_{max1} = (\log\alpha)/\beta$. Note that the probability of having an event with potency greater than or equal to P_{max1} is finite, $\Pr\,(\geq P_{max1}) = P_{min}^{\beta}/\alpha$, where P_{min} is the lowest threshold potency

selected to fit the power law. The probability of having an event with potency not smaller than P is $\Pr(\geq P) = N(\geq P)/N(\geq P_{min}) = P_{min}^{\beta} P^{-\beta}$. The number of events within the potency range of (P_1, P_2) is $N(P_1, P_2) = \alpha\left(P_1^{-\beta} - P_2^{-\beta}\right)$ and the probability of having a seismic event within the potency range (P_1, P_2) is given by $\Pr(P_1, P_2) = P_{min}^{\beta}\left(P_1^{-\beta} - P_2^{-\beta}\right)$. The probability density function for the OE relation is $f(P) = \beta P_{min}^{\beta} P^{-\beta-1}$ and the mean value of the distribution $\langle P\rangle = P_{min}\beta/(\beta-1)$ is finite for $\beta > 1$. The potency release by seismic events within the potency range P_1 and P_2 is $P(P_1, P_2) = N(P_1, P_2)\int_{P_1}^{P_2} Pf(P)dP / \int_{P_1}^{P_2} f(P)dP$. For $\beta < 1$, one can integrate from $P_1 = 0$ to a finite potency $P(0, P_2) = \alpha\beta P_2^{1-\beta}/(1-\beta)$. For $\beta = 1$ one can integrate within the finite potency range, $P(P_1, P_2) = \alpha \ln(P_2/P_1)$ and for $\beta > 1$ it can be integrated from a finite potency to infinity, $P(P_1, \infty) = -\alpha\beta P_1^{1-\beta}/(1-\beta)$. For $\beta < 1$ the following ratio quantifies the portion of missing potency below P_{min}.

$$\frac{P(0, P_{min})}{P(P_{min}, P_{max})} = \frac{P_{min}^{1-\beta}}{P_{max}^{1-\beta} - P_{min}^{1-\beta}}. \tag{2}$$

In general, the ratio (2) increases with an increase in the β-value and with a decrease in the P_{max}. Theoretically that portion can be as low as a fraction of a percent for a large P_{max} and for a relatively low β-value or, it may exceed 100% in the opposite case, see Figure 3.

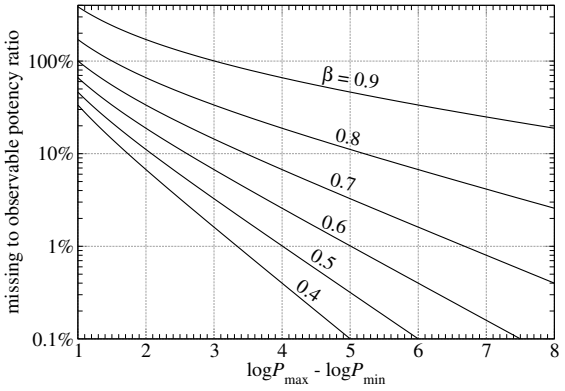

Figure 3: Missing potency ratio.

Upper-truncated power law. The UT relation is a version of OE with a hard upper limit on potency, P_{max}, such that $\Pr(> P_{max}) = 0$. The number of events with potency not smaller than P is

$$N(\geq P) = \alpha\left(P^{-\beta} - P_{max}^{-\beta}\right). \tag{3}$$

The probability $\Pr(\geq P) = \left(P^{-\beta} - P_{max}^{-\beta}\right)/\left(P_{min}^{-\beta} - P_{max}^{-\beta}\right)$ and of having an event within a potency range (P_1, P_2) is given by $\Pr(P_1, P_2) = \left(P_1^{-\beta} - P_2^{-\beta}\right)/\left(P_{min}^{-\beta} - P_{max}^{-\beta}\right)$. The probability density function is $f(P) = \beta P^{-\beta-1}/\left(P_{min}^{-\beta} - P_{max}^{-\beta}\right)$ and the mean value of the distribution is $\langle P\rangle = [\beta/(1-\beta)]\left(P_{max}^{1-\beta} - P_{min}^{1-\beta}\right)/\left(P_{min}^{-\beta} - P_{max}^{-\beta}\right)$. The variance is defined as $Var(P) = \langle P^2\rangle - (\langle P\rangle)^2$ and the skewness is $\gamma(P) = \left[\langle P^3\rangle - 3\langle P\rangle Var(P) - (\langle P\rangle)^3\right]/[Var(P)]^{3/2}$, where $\langle P^n\rangle = [\beta/(n-\beta)]\left(P_{max}^{n-\beta} - P_{min}^{n-\beta}\right)/\left(P_{min}^{-\beta} - P_{max}^{-\beta}\right)$, for n=2, 3. The equations for potency production are similar to the OE distribution, with the exception that P_2 can only go to P_{max}.

Information Entropy and β. Following *Shannon*'s second paper, the continuous, as opposed to the discrete, information entropy of the probability density function

of potency P can be written as $H\left[f\left(P\right)\right]=\int_0^\infty f\left(P\right)\log[1/f\left(P\right)]dP$, where $f\left(P\right)$ is the probability density function. The continuous entropy is not a limit of the discrete entropy when the bin size goes to zero. The entropies of continuous distributions have most, but not all, of the properties of the discrete case. There is one important difference between the continuous and discrete entropies. In the discrete case the entropy measures the randomness of the variable in an absolute way. The continuous formulation measures it relative to the coordinate system and the entropy can be negative. It is not important, though, if one is interested in the differences or in the rate of change between two or more entropies, since they are independent of the frame of reference (*Shannon*, 1948).

The $\log\left(1/f\left(P\right)\right)$ is the information content of event P with probability $f\left(P\right)$ and, if $f\left(P\right)$ is high then knowledge that event P occurred gives very little information, since it had a high probability of occurrence to start with. The information entropy is therefore an average information weighted by the probability of each event. Events with either very high or very low probabilities do not contribute significantly to the information entropy. H reaches its maximum value if all states are equally probable and it decreases as the uniformity of the probability distribution is being eroded. Therefore H measures the amount of uncertainty in a given distribution, which is a measure of randomness and unpredictability. For the UT distribution

$$H=2.3\beta\left(1+\beta\right)A-B\left[2.3\beta\log\left(-\beta\left(P_{min}P_{max}\right)^{\beta}/B\right)-\beta-1\right]/\left(2.3\beta B\right), \qquad (4)$$

where $A=\left(P_{min}^{\beta}\log P_{max}-P_{max}^{\beta}\log P_{min}\right)$, $B=P_{min}^{\beta}-P_{max}^{\beta}$ and $2.3=\ln\left(10\right)$. For the OE distribution $H=\log\left(P_{min}/\beta\right)+0.434(1/\beta+1)$.

From both equations it follows that uncertainty, or unpredictability, increases with decreasing β, more so in case of the OE see Figure 4. Tests on three data sets described below show that the most predictable values of P are within the data set B, followed by A and then C.

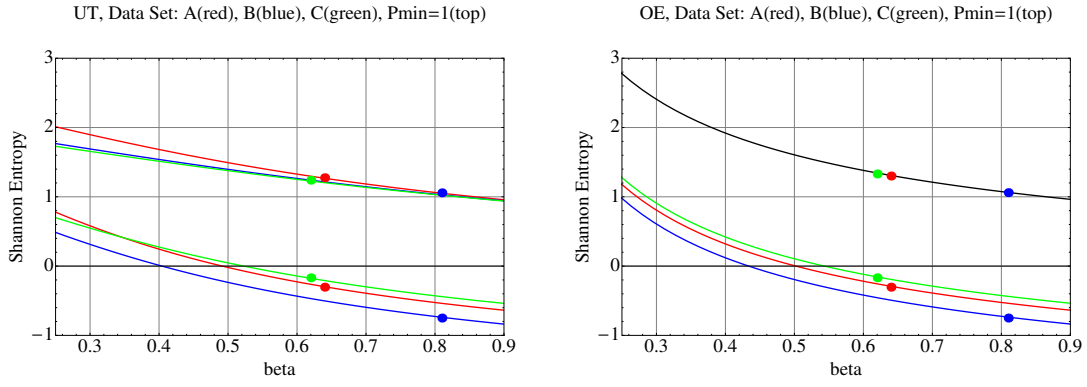

Figure 4: Information entropy H for UT *(left)* and OE *(right)* distributions as a function of β for the three data sets: A (red), B (blue) and C (green). The bottom three lines are for P_{min} as in the data (note the negative range for H) and the top three lines *(left)* and one collapsed top line *(right)* are for $P_{min}=1$.

3 Rock Mass Heterogeneity, Stress, Stiffness and β.

For a data set that obeys the power law size distribution the exponent β is a statistical measure of the ratio of small to large events, and it decreases as the portion of the intermediate and large events increases. This power law is well observed for small and intermediate magnitude range events that occur within a given seismogenic volume over longer period of time.

In some cases, however, data points on the cumulative frequency plot indicate a double slope convex or concave character. One possible explanation of such deviations is the change in the sensitivity of the monitoring system during acquisition of data. Another possibility is that the data is generated by two spatially separated processes with different size distributions. The concavity, see Figure 5, may be generated by a combination of high activity of low magnitude events induced by mining excavation(s) with a few larger events caused by an existing geological structure. This behaviour is frequently a function of the spatial and/or temporal data selection.

The more frequently observed convexity, see Figure 9, is caused by a deficit of larger events and may indicate that the size distribution hazard is contained.

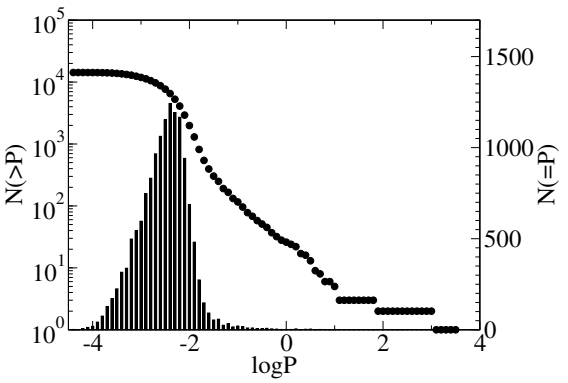

Figure 5: An example of a concave power law data set recorded at WH2# during one year period in the cumulative *(dots)* and non-cumulative forms *(vertical bars)*.

In general, the exponent β is found to be influenced by the degree of rock mass heterogeneity, the average level of stress and the stiffness of the system.

The rock mass heterogeneity depends on the spatial distribution of sizes and distances between strong and/or stressed and weak and/or destressed patches of rock where seismic sources may nucleate and be stopped. An increase in rock heterogeneity results in a higher β, since it is more likely that the initiated rupture be stopped by a soft or hard patch before growing into a larger event (*Mogi*, 1962; *Mori and Abercombie*, 1997). *Scholz* (1968) stated that the β-value varies inversely with stress. The reasoning that β tends to be lower in high stress areas is based on a similar argument to heterogeneity, namely, that rupture once initiated grows larger in a high stress regime. In his paper *Scholz*, 1968 also argues that *Mogi*, 's experiments were done in the low frequency range and therefore the conclusions are open to question. Later Kiyoo Mogi repeated his measurements in high frequencies and with exceptionally high dynamic range and reconfirmed his initial results (*Mogi*, 1980; *Mogi*, 1981). He also conducted tests under constant compressive stress and observed a gradual decrease in β until the main rupture (see also *Mogi*, 2007, pages 250 - 261).

Frohlich and Davis (1993), *Schorlemmer et al.* (2005) and *Gulia and Wiemer* (2010) show that the areas characterised by reverse faulting have lower β-values than the zones with strike-slip, and that the highest values of β were associated with normal faulting. Given that thrust faults tend to be under higher stress than normal faults they argue that β depends inversely on differential stress.

Experimental study on rock samples of equal degrees of heterogeneity in triaxial conditions has shown a decrease in β of acoustic emission events with both the differential stress and the confining pressure, during all stages of stress-strain regime, including the post peak strain softening (e.g. *Amitrano*, 2003).

Stiffness measures the rigidity of a system, i.e. its ability to resist deformation in response to an applied load. It scales positively with the ratio of the applied stress (or force) to the induced strain (or displacement). *Mendecki and van Aswegen*, 1998 and *van Aswegen and Mendecki*, 1999 observed a higher β in stiffer systems. These observations do not contradict reports on decreasing β with increasing stress during the strain hardening regime, since there is a general loss of stiffness with increasing stress. However, in a strain softening regime, where the strength is decreasing with increasing strain, stress is lower but we observed lower β.

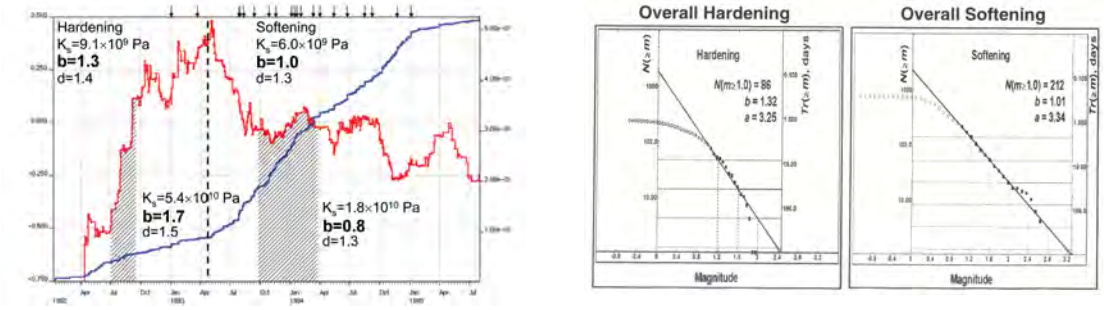

Figure 6: *(Left)* Time plot of $\log(EI)$ in red and cumulative V_A in blue, during WH6 shaft pillar extraction. Arrows on top indicate the occurrence of large events and K_s is the stiffness modulus. *(Right)* Cumulative magnitude-frequency plot for the hardening and softening regimes.

Figure 6 shows the time evolution of energy index EI (a proxy for stress) and the cumulative apparent volume, $V_A = M/\sigma_A$, (a proxy for deformation) during shaft pillar extraction at the Western Holding gold mine. Mining was at a depth of 1400 m progressing from the centre of the pillar to the outer perimeter. Due to the similarity of this layout to the triaxial lab rock failure test one would expect a hardening phase – nonlinear stress increase to its peak, followed by a softening of the pillar and an increased rate of deformation. Other parameters depicted in Figure 6 are: seismic stiffness $K_s = \sigma_s/\epsilon_s$, the ratio of seismic stress σ_s and seismic strain (*Kostrov and Das*, 1988), the b-value in the Gutenberg-Richter relation and d which is the slope of the $\log E = d \log P + c$ relation. Note that almost all events larger than $\log E$=7.5 occurred after the all time peak in EI.

4 Mining Factors and Seismic Hazard

Hazard factors. Seismic hazard in mines is positively correlated with the following natural factors: virgin rock stresses, which is a combination of depth and tectonic stress, mechanical strength of the rock, the degree of homogeneity, or smoothness, of the rock mass that includes the presence and the nature of geological features – specifically those with shear strength comparable to the shear stresses induced by mining excavations.

In addition there is a number of mining related factors that may exacerbate the intensity of the seismic rock mass response to mining, among them: the extraction ratio, the extent of the mined-out area, the rate and the spatial and temporal sequence of extraction, additional stress induced by the adjacent mining, and the smoothness of the mine layout itself and in relation to the geological structures. Smoothness here is defined by the dimensionality of the object, as measured by its fractal dimension – the lower the fractal dimension the smoother the object.

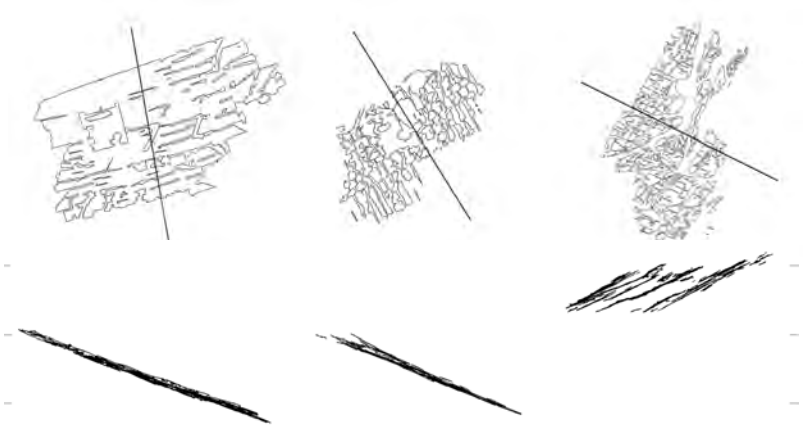

Figure 7: Mine layouts in plan *(top)* and in section *(bottom)* associated with data set A with fractal dimension $D_{ml} = 1.67$ (left), B with fractal dimension $D_{ml} = 1.68$ (center) and C with fractal dimension $D = 1.71$ (right).

The objective of this section is to show the complex relation between the natural factors, mining factors and related seismic hazard for the three data sets. It also demonstrates the difficulties in utilising the size distribution parameters in rating seismic hazard.

Data sets. Data sets A, B and C were collected over the same two year period (Δt = 678 days), all related to tabular mining with principal vertical stresses but with different geological structures, mining layouts, extraction ratios, depths and different rates of mining. The data set A is associated with long-wall mining of highly extracted tabular reef and data set B is related to sequential grid mining, see *Vieira et al.*, 2001 for a review of these mining methods. In both cases, A and B, the rock extraction took place at practically the same depth of 3300 m. Data set C is related to the scattered

mining imposed by the presence of larger geological structures at an average depth of 1755 m, see Figure 7. A simple numerical elastic model shows that due to the higher extraction ratio the mean vertical stress calculated over the un-mined areas in mine A is 1.7 times higher than in mine B.

Hazard rating. The depth of mining, the volume mined, the rate of mining and the approximate extraction ratio are listed in Table 1. The relative hazard rating from (1) – the highest to (3) – the lowest, imposed by the author for each parameter are also quoted, where applicable.

Table 1: Mining factors with hazard rating in parentheses.

Parameter	Data Set A	Data Set B	Data Set C
Weighted depth of extraction, m	3294 (1)	3287 (2)	1755 (3)
Volume mined, V_m, m^3	93190 (3)	418271 (1)	292677 (2)
Rate of mining, m^3/day	137 (3)	617 (1)	432 (2)
Approximate extraction ratio, %	80 (1)	70 (2)	60 (3)

Because the rate of rock extraction that drives the seismic response in mines varies, the most conclusive parameters are those incorporating V_m, see Table 2. The highest production, the production rate and the highest seismic potency release is associated with data set B. However, the highest observed potency release per unit of volume mined, $\sum P/V_m$, is associated with data set A. Compared to A and B the seismic potency release for data set C is low. Note, that the production in B is 4.5 times higher than in A, however, the potency release per day is only 1.6 time higher, and the potency release per unit of volume mined 2.8 times lower. Clearly the most informative parameter of the inherent hazard is $\sum P/V_m$, and if it is unacceptably high then the slower pace of mining only delays the inevitable.

Table 2: Observed hazard related parameters, with hazard rating in parentheses.

Parameter	Data Set A	Data Set B	Data Set C
Two largest observed events	3.4; 3.0 (1)	2.7; 2.6 (2)	2.6; 2.5 (3)
$N_{obs}(\geq \log P{=}2)$	31 (1)	29 (2)	15 (3)
$N_{obs}(\geq \log P{=}1.5)$	84 (2)	149 (1)	46 (3)
V_m/ $N_{obs}(\geq \log P{=}2)$, m^3	3006 (1)	14423 (2)	19512 (3)
$V_m/N_{obs}(\geq \log P{=}1.5)$, m^3	1109 (1)	2807 (2)	6363 (3)
$\sum P$/day, [m^3/day]	28.53 (2)	44.91 (1)	12.58 (3)
$\sum P/V_m$	0.209 (1)	0.074 (2)	0.03 (3)

The cumulative graphs of the volume mined vs time, the potency release vs time and the potency release vs volume mined are shown in Figure 8 left, centre and right respectively. The potency release vs volume mined is self-explanatory and rates the absolute seismic hazard for the three data sets clearly: the highest is A (1), the second highest is B (2) and the lowest of the three is C (3). The largest observed events to date rated hazard in the same sequence, but they're not forward looking parameters, hence of limited utility.

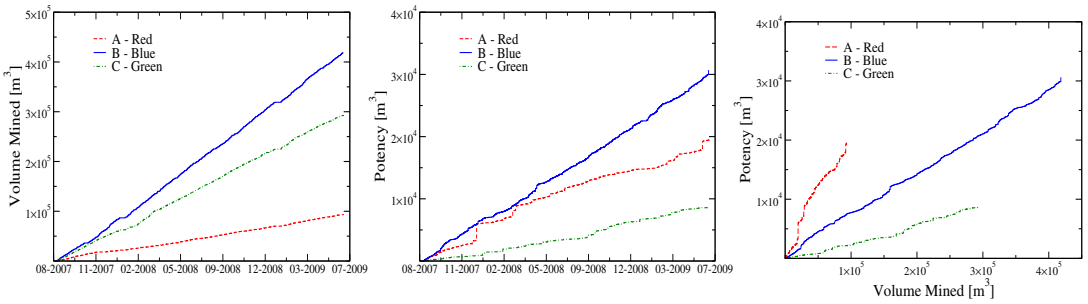

Figure 8: All cumulative: volume mined versus time *(left)*, potency release versus time *(centre)* and potency release versus volume mined *(right)*.

Layout, sequence of mining and hazard. To gain insight into the influence of the mine layout on seismic hazard we estimated their respective fractal dimensions. Fractals appear similar at any scale of observation. In mathematical terms, fractal objects exhibit fractional dimensionality, that is, they are neither lines, nor surfaces or volumes. Their dimension falls in between the classical dimensions of Euclidean geometry. An object is fractal when its length L is a function of the length λ of the measuring device, $L \sim \lambda^{1-D}$, where D is the fractal dimension (*Mandelbrot*, 1967, 1975). If $N(\lambda)$ is the number of cubes of size λ needed to cover the object then the box counting fractal dimension of an object can be estimated by $D = \ln N(\lambda)/\ln(1/\lambda)$ (*Barnsley*, 1988). Fractal dimension increases with the degree of irregularity, or raggedness of the object. The lowest fractal dimension of mine layout, $D_{ml} = 1.67$ is associated with long-wall mining, followed by sequential grid, $D_{ml} = 1.68$, and the roughest is the scattered mining imposed by the presence of geological structures $D_{ml} = 1.81$. This sequence could easily be inferred just by looking at the smoothness of lines in Figure 7.

Table 3: Mining factors, with hazard rating in parentheses.

Parameter	Data Set A	Data Set B	Data Set C
D_{ml} of mine layout	1.67 (1)	1.68 (2)	1.71 (3)
D_{sxy} of epicenters	1.60 (2)	1.49 (1)	1.61 (3)
D_{ste} of space-time extraction	1.84 (1)	1.92 (2)	2.20 (3)
D_{sxyt} of epicenters and time	1.84 (3)	1.71 (1)	1.83 (2)

Having coordinates and the dates and times of panel extraction we connected lines between consecutively extracted panels and calculated the fractal dimension of such a spatial and temporal graph, D_{ste}. The smoothest sequence of mining, $D_{ste} = 1.84$, is associated with mine A, then B with $D_{ste} = 1.92$, and the roughest by mine C with $D_{ste} = 2.20$. By connecting lines between consecutive seismic events we created an image of the sequence of seismic activity and then calculated its fractal dimension. This exercise was limited to the (x, y, t) domain since the flat distribution of seismic stations made the z-coordinates less reliable, specifically at the fringes of the network. Results and the relative hazard ratings are given in Table 3. They show

that seismic activity does not follow mining exactly. One may speculate that the high stress and high rate of mining associated with data set B aligned most events with the excavation faces lowering the fractal dimension of their spatial distribution, but this has not been tested numerically.

There is also a negative correlation between the fractal dimension of the epicenters and time of events, D_{sxyt}, and β, see Tables 3 and 4. There are reports stating the positive correlation between the b-value and earthquakes, e.g. *Aki* (1981), *King* (1983), *Wyss et al.* (2004), *Chen et al.* (2006), but mainly for a single fracturing or a single fault processes. *Hirata* (1989) reported a negative correlation due to different fault systems and *Henderson et al.* (1999) for induced seismicity where they show a negative correlation for high loading rates and a positive correlation for slowly loaded systems. *Amitrano* (2003) also reported negative correlation stating that diffused damage is associated with low β whereas localized damage is associated with high β. The data set B has the highest loading rate of all three and the lowest fractal dimension, followed by data set C, and the lowest loading rate and the highest fractal dimension is associated with data set A.

Size distribution parameters. The cumulative potency-frequency plots that include the inter-event volumes mined as opposed to the recurrence times are shown in Figure 9.

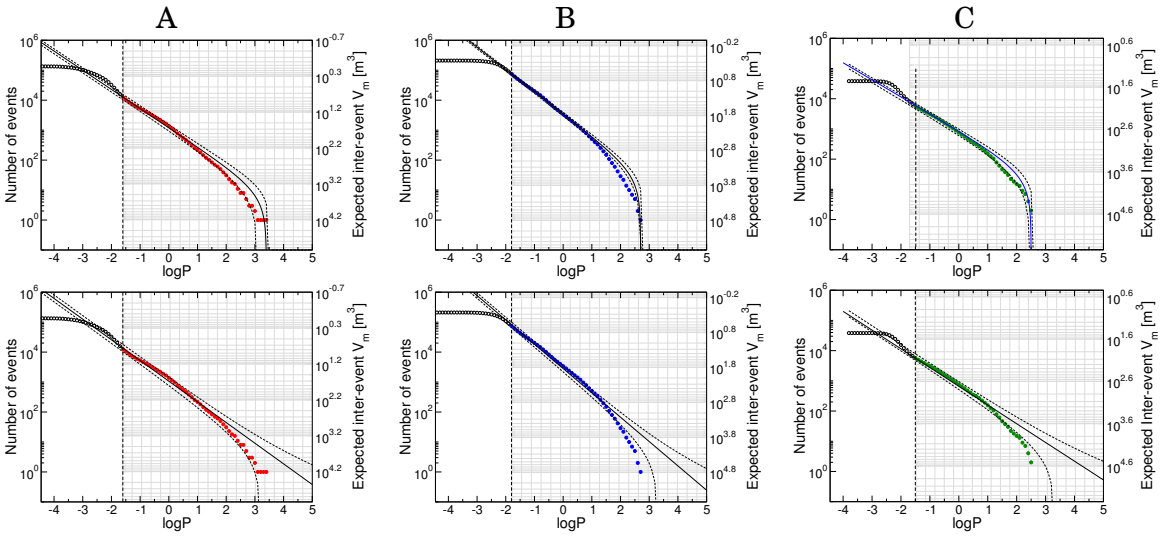

Figure 9: Cumulative potency-frequency plots for the three data sets. The convex curve in the top row represents the UT fit for $\log P_{max}$=$\log P_{maxo}$, where P_{maxo} is the largest observed event to date, and the straight line in the bottom row represents the OE power law fit. The dotted lines show the 95% confidence intervals calculated assuming that the number of events in each potency interval comes from the Poisson distribution.

An increase in the cumulative number of events below $\log P$=$-$1.5 in the data

sets A and C is the result of an uneven network sensitivity enhanced by development blasts recorded as seismic events. The 95% confidence intervals show that the UT relation fits data better than the OE one and that of all three, data set A is the closest to the OE relation.

In general, seismic hazard should scales positively with α, and with $\log P_{max1}$ and negatively with β and recurrence times. The Table 4 shows that none of the traditional size distribution parameters, namely α, β or $P_{max1} = \alpha^{1/\beta}$, succeeded in rating seismic hazard in the three data sets consistently and reliably. The only parameter that did succeed is the inter-event volume mined, $\bar{V}_m\,(\geq P) = V_m/N\,(\geq P)$, which rated hazard appropriately for both $\log P$=2.0 and $\log P$=1.5.

Table 4: Size distribution parameters, with hazard rating in parentheses.

Model Parameters	Data Set A	Data Set B	Data Set C
α_{OE}; α_{UT}	1202; 1318 (2)	2818; 3467 (1)	724; 813 (3)
β_{OE}; β_{UT}	0.64; 0.59 (2)	0.81; 0.74 (3)	0.62; 0.56 (1)
$\log P_{max1}$=$(\log \alpha_{OE})/\beta_{OE}$	4.8 (1)	4.2 (3)	4.6 (2)
$\bar{t}(\geq \log P$=2.0), days	9.2 (2)	8.5 (1)	20.41 (3)
$\bar{t}(\geq \log P$=1.5), days	4.3 (2)	2.9 (1)	7.6 (3)
$\bar{V}_m(\geq \log P$=2.0), m^3	1258 (1)	5230 (2)	8811 (3)
$\bar{V}_m(\geq \log P$=1.5), m^3	587 (1)	1784 (2)	3284 (3)

While $\log P_{max1}$ rated data set A as the highest hazard, it failed the sequence badly. It demonstrates the ill-suitability of $\log P_{max1}$ as derived from the OE relation as the main measure of seismic hazard. When the largest observed events are as predicted by the $\log P_{max1}$ in the OE relation, it is inappropriate to infer that this is the largest possible event (see *Frohlich*, 1998). The fact that the data follow the OE power law indicates the potential for even larger events. Only when the largest observed events are significantly smaller than that predicted by the OE relation, as in this case, can one infer that the size distribution hazard may be contained. The inter-event times or the recurrence times $\bar{t}\,(\geq P)$ here are also misleading.

5 Record Breaking Events Induced by Mining

As mentioned above the $\log P_{max1}$ is not a reliable measure of seismic hazard and it does not answer the two important questions: (1) what is the size of the largest possible event and, (2) what is the size of next record breaking event.

The size of the largest possible event induced by mining scales approximately with the characteristic size of the mine, L, and with the extent of the major geological structures influenced by mining. If we assume the upper-bound relation between the maximum magnitude and the linear size of the mine as, $m_{max} = 2.0 \log L - 2.0$ (*McGarr and Fletcher, 2002*), then for $L = 1500$ m an average m_{max}=4.3 or, according to *Hanks and Kanamori* (1979), $\log P_{max} = 1.5 m_{HK} - 1.38 = 5.1$. For $L = 2{,}500$ m

the m_{max}=4.8 and $\log P_{max}$=5.8. However, there are many mines with characteristic dimension $L \geq$ 1,500 m that did not generate seismic events of that size.

The expected size of the next record breaking event can, in some cases, be estimated from the record breaking theory (e.g. *Tata*, 1969; *Chandler*, 1952; *Glick*, 1978; *Nevzorov*, 2001, *Dargahi-Noubary*, 1990; *Van Aalsburg et al.*, 2010). In a sequence $\{P_j\}_{j=1,2,}$ of real random variables a record high occurs at r if $P_r = \max_{j \leq r} \{P_j\}$. Obviously P_1 is always a record. If events are independent and identically distributed, the probability that a record high, or low occurs at j is $1/j$ and probability that it is not is $(j-1)/j$. The expected mean number of records high (or low), $\langle N_{rb} \rangle$ is $\sum_{j=1}^{n} (1/j)$, which for large n can be approximated by $\langle N_{rb}(n) \rangle = \sum_{j=1}^{n} \frac{1}{j} \approx \ln(n) + 0.577215$. The variance $Var(N_{rb}) = \sum_{j=1}^{n} (1/j) - \sum (1/j^2) \approx \ln(n) - 1.0677$. The record sequence is distinctly non-stationary: with increasing time, i.e., it becomes exponentially harder to beat the current record, see Table 5.

Table 5: The expected number of records in n independent observations.

n	10^1	10^2	10^3	10^4	10^5
$\langle N_{rb} \rangle$	2.93	5.19	7.49	9.8	12.1
$\sqrt{Var}$	1.17	1.88	2.42	2.85	3.23

To estimate the size of the next record breaking event in our data sets we used the UT potency frequency distribution to secure the finite mean for the case $\beta < 1$. The parameter P_{max} of the UT distribution can be taken as the maximum observed event to date plus the maximum expected jump in record breaking events to date

$$\log P_{max} = \log P_{maxo} + \triangle \log P_{max}. \tag{5}$$

The maximum expected jump, $\triangle \log P_{max}$, can be estimated as a truncation point of the distribution of the previous jumps (*Cooke*, 1979)

$$\triangle \log P_{max} = 2 \max(\Delta \log P_{maxo}) - 0.63 \sum_{j=0}^{n-1} \frac{\max(\Delta \log P_{maxo-j})}{e^j}, \tag{6}$$

where $\max(\Delta \log P_{maxo})$ is the maximum observed jump in the history of records.

The value of the first record breaking event is the potency of the first event to occur which, most likely, is the mean value of the UT potency frequency distribution, $P_{rb(1)} = \beta/(1-\beta) \left(P_{max}^{1-\beta} - P_{min}^{1-\beta}\right) / \left(P_{min}^{-\beta} - P_{max}^{-\beta}\right)$. The value of the second record breaking event is the mean value of that portion of the UT distribution that lies beyond the first record, $P_{rb(2)} = \int_{P_{rb(1)}}^{\infty} Pf(P)\,dP / \int_{P_{rb(1)}}^{\infty} f(P)\,dP$, and recursively the kth record is

$$P_{rb(k)} = \frac{\beta}{1-\beta} \left(\frac{P_{max}^{1-\beta} - P_{r(k-1)}^{1-\beta}}{P_{r(k-1)}^{-\beta} - P_{max}^{-\beta}} \right), \quad \text{for} \quad k = 2, 3, ... \tag{7}$$

where $P_{r(k-1)}$ is the potency of the previous record breaking event and the $P_{max}^{1-\beta}$ is given by $\log P_{max} = \log P_{maxo} + \triangle \log P_{max}$. If observations are independent and

identically distributed, then the number of records calculated forward should be equal to the number of records calculated backwards, e.g. the data set A, see Table 6. For the data set B and C the number of forward records is considerable greater which is symptomatic of an increasing future hazard.

Table 6: Record statistics.

Record Parameters	Data Set A	Data Set B	Data Set C
Number of events $N \geq \log P_{min}$	11507	81812	5376
Expected number of records, $\langle N_{rb} \rangle$	9.93	11.89	9.17
Standard deviation, $\sqrt{Var}$	2.88	3.2	2.74
Observed number of forward records	7	14	11
Observed number of backward records	5	4	5
Max. observed record jump	0.8	0.6	0.5
Average jump of record events	0.4	0.2	0.2
Expected next record, Eq.(7)	3.86	3.05	2.79
Estimated upper limit, Eq.(5)	4.39	3.45	3.11

Figure 10 shows the history of the record breaking events in the volume mined domain for the data sets A (left), B (centre) and C (right). The predicted ranges of the next record breaking events calculated by the Equations (7) and (5) are shown as grey bands. These predictions, like all seismic hazard parameters quoted before, were calculated using data up to the last observed record – a black dot at the end of the solid stepping line. The next record in each case is shown as a cross following the dotted stepping line. There were no new records in the data set A, where rock extraction was suspended for some time and resumed later at a low rate. The next record breaking event in the data set B occurred 197 days and 126,778 m^3 of volume mined later and measured $\log P$=2.9, which is 0.15 less than predicted. The next record in the data set C occurred 540 days and 219,678 m^3 later and measured $\log P$=3.1, which is 0.05 above the estimated range.

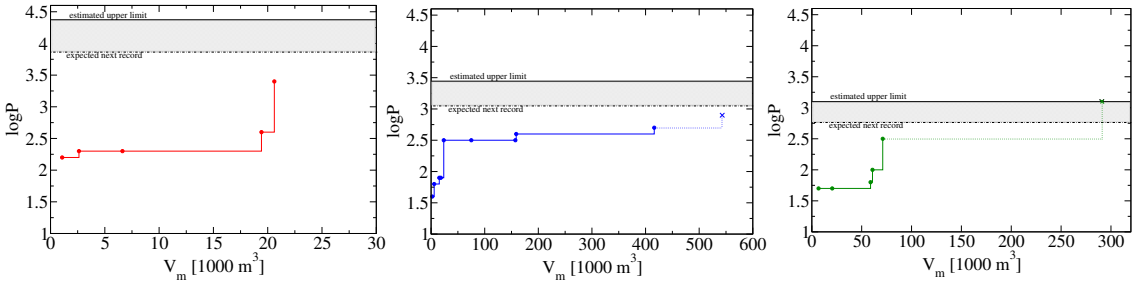

Figure 10: History of the record breaking events in the volume mined domain for the data sets A *(left)*, B *(centre)* and C *(right)*. The predicted ranges for the next record are shown as a grey band and the next observed record as a little cross at the end of the dotted stepping line.

If the exponent β of the potency-frequency relation is constant then the Equation (7) is discrete and one can estimate the magnitude of the next record breaking event only after the "current" record has occurred. The data analysed to date shows that in mines β may have a relatively persistent trend, either way. Over the longer term, however, as mining progresses the stiffness of the rock mass is being degraded and β tends to drop (*Mendecki*, 2008). Therefore, the Equation (7) can be expressed as a function of volume mined by replacing β by $\beta\,(V_m)$, and then one can estimate the magnitude of the next record breaking event every time β changes or, by extrapolating the observed relationship between β and the V_m, one can forecast future records for a different production scenarios.

Acknowledgment

A part of the material related to the fractal dimension and seismic hazard was presented by the author in a keynote lecture at the 7th International Symposium on Rockburst and Seismicity in Mines, Dalian, China. I thank Cornel du Toit for stimulating discussions on different aspects of the paper.

This project is a part of the Mine Seismology Research Programme sponsored by Anglo American Platinum, South Africa; Anglo Gold Ashanti, South Africa; BHB Billiton Nickel West, Australia; El Teniente, Chile; Gold Fields, South Africa; Harmony, South Africa; LKAB, Sweden; Newcrest Mining Australia.

References

Aki, K. (1981), A probabilistic synthesis of precursory phenomena, in *Earthquake Prediction: An International Review*, edited by D. W. Simpson and P. G. Richards, Maurice Eving, pp. 566–574, American Geophysical Union, Washington D. C.

Amitrano, D. (2003), Brittle-ductile transition and associated seismicity: Experimental and numerical studies and relationship with the b-value, *Journal of Geophysical Research*, *108 (B1)*(2044), 1–15, doi:10.1029/2001JB000680.

Barnsley, M. F. (1988), *Fractals Everywhere*, Academic Press.

Chandler, K. N. (1952), The distribution and frequency of record values, *Journal of the Royal Statistical Society, Series B (Methodological)*, *14*(2), 220–228.

Chen, C.-C., W.-C. Wang, Y.-F. Chang, Y.-M. Wu, and Y.-H. Lee (2006), A correlation between the b-value and the fractal dimension from the aftershock sequence of the 1999 Chi-Chi, Taiwan, earthquake, *Geophysical Journal International*, *167*(3), 1215–1219.

Christensen, K., L. Danon, T. Scanlon, and P. Bak (2002), Unified scaling law for earthquakes, *PNAS*, *99*(1), 2509–2513.

Cooke, P. (1979), Statistical inference for bounds of random variables, *Biometrica*, *66*(2), 367–374.

Cornell, C. A., and E. H. Vanmarcke (1969), The major influences on seismic risk, in *Proceedings 4th World Conference on Earthquake Engineering, Santiago, Chile*, pp. 69–83.

Cosentino, P., V. Ficarra, and D. Luzio (1977), Truncated exponential frequency-magnitude relationship in earthquake statistics, *Bulletin of the Seismological Society of America*, *67*(6), 1615–1623.

Dargahi-Noubary, G. R. (1990), Seismic hazard assessment using the theory of records, *Natural Hazards*, *3*(2), 161–171.

Frohlich, C. (1998), Does maximum earthquake size depend on focal depth?, *Bulletin of the Seismological Society of America*, *88*(2), 329–336.

Frohlich, C., and S. D. Davis (1993), Teleseismic b values. Or, much ado about 1.0, *Journal of Geophysical Research*, *98*(B1), 631–644.

Glick, N. (1978), Breaking records and breaking boards, *The American Mathematical Monthly*, *85*(1), 2–26.

Gulia, L., and S. Wiemer (2010), The influence of tectonic regimes on the earthquake size distribution: A case study for Italy, *Geophysical Research Letters*, *37*(L10305), 1–6, doi:10.1029/2010GL043066.

Hanks, T. C., and H. Kanamori (1979), A moment magnitude scale, *Journal of Geophysical Research*, *84*, 2348–2350.

Henderson, J. R., D. J. Barton, and G. R. Foulger (1999), Fractal clustering of induced seismicity in The Geysers geothermal area, California, *Geophysical Journal International*, *139*(2), 317–324, doi:10.1046/j.1365-246x.1999.00939.x.

Hirata, T. (1989), A correlation between the b value and the fractal dimension of earthquakes, *Journal of Geophysical Research*, *94*(B6), 7507–7514.

Jackson, D. D., and Y. Y. Kagan (2006), The 2004 Parkfield earthquake, the 1985 prediction, and characteristic earthquakes: Lessons for the future, *Bulletin of the Seismological Society of America*, pp. S397–96S409, doi:10.1785/0120050821.

Jensen, H. J. (1998), *Self-Organized Criticality: Emergent Complex Behavior in Physical and Biological Systems*, Cambridge Lecture Notes in Physics 10, first ed., Cambridge University Press.

Kagan, Y. Y., D. D. Jackson, and R. J. Geller (2012), Characteristic earthquake model, 1884-2011, R.I.P, *arXiv:1207.4836v1*, *1*, 1–7.

Kijko, A., and T. Stankiewicz (1987), Bimodal character of the distribution of extreme seismic events in Polish mines., *Acta Geophysica Polonica*, *35*, 491–506.

King, G. (1983), The accommodation of large strains in the upper lithosphere of the earth and other solids by self-similar fault systems: The geometrical origin of b-value, *Pure and Applied Geophysics*, *121*(5-6), 761–815, doi:10.1007/BF02590182.

Kostrov, B. V., and S. Das (1988), *Principles of Earthquake Source Mechanics*, Cambridge University Press.

Kwiatek, G., K. Plenkers, M. Nakatani, Y. Yabe, and G. Dresen (2010), Frequency-magnitude characteristics down to magnitude -4.4 for induced seismicity recorded at Mponeng gold mine, South Africa, *Bulletin of the Seismological Society of America*, *100*(3), 1165–1173.

Main, I. G., and P. W. Burton (1984), Physical links between crustal deformation, seismic moment and seismic hazard for regions of varying seismicity, *Geophys. J. R. Astron. Soc.*, *79*(2), 469–488.

Mandelbrot, B. B. (1967), How long is the coast of Britain? Statistical self-similarity and fractional dimension, *Science*, *156*, 636–638.

McGarr, A., and J. B. Fletcher (2002), Mapping apparent stress and energy radiation over fault zones of major earthquakes, *Bulletin of the Seismological Society of America*, *92*(5), 1633–1646.

Mendecki, A. J. (1993), Real time quantitative seismology in mines: Keynote Address, in *Proceedings 3rd International Symposium on Rockbursts and Seismicity in Mines, Kingston, Ontario, Canada*, edited by R. P. Young, pp. 287–295, Balkema, Rotterdam.

Mendecki, A. J. (1997), Quantitative seismology and rock mass stability, in *Seismic Monitoring in Mines*, edited by A. J. Mendecki, 1 ed., chap. 10, pp. 178–219, Chapman and Hall, London.

Mendecki, A. J. (2008), Forecasting seismic hazard in mines, in *Proceedings 1st Southern Hemisphere International Rock Mechanics Symposium, Perth, Australia*, edited by Y. Potvin, J. Carter, A. Diskin, and R. Jeffrey, pp. 55–69, Australian Centre for Geomechanics.

Mendecki, A. J., and E. C. Lötter (2011), Modelling seismic hazard for mines, in *Australian Earthquake Engineering Society 2011 Conference, Barossa Valley*.

Mendecki, A. J., and G. van Aswegen (1998), System stiffness and seismic characteristics - A case study, in *International Workshop on Frontiers in Monitoring Science and Technology for Earthquake Enviroments, Japan*, edited by M. Ando, pp. F4–2.

Mendecki, A. J., G. van Aswegen, J. N. R. Brown, and P. Hewlett (1988), The Welkom seismological network, in *Proceedings 3rd International Symposium on Rockbursts and Seismicity in Mines, Minneapolis, USA*, edited by C. Fairhurst, pp. 237–244, Balkema, Rotterdam, 1990.

Mogi, K. (1962), Magnitude frequency relations for elastic shocks accompanying fractures of various materials and some related problems in earthquakes, *Bulletin Earthquake Research Institute of Tokyo University*, *40*, 831–853.

Mogi, K. (1980), Amplitude-frequency relationship od acoustic emission events, *Selsmological Society of Japan (in Japanese).*, p. 176.

Mogi, K. (1981), Earthquake prediction program in Japan, in *Earthquake Prediction*, edited by D. W. Slmpson and P. G. Richards, Maurice Ewing Series 4, pp. 635–666, American Geophysical Union.

Mogi, K. (2007), *Experimental Rock Mechanics*, 361 pp., Taylor and Francis.

Mori, J., and R. E. Abercombie (1997), Depth dependence of earthquake frequency-magnitude distribution in California: Implications for rupture initiation, *Journal of Geophysical Research*, *102*(B7), 15,081–15,090.

Nevzorov, V. B. (2001), *Records: Mathematical Theory*, *Translations of Mathematical Monographs*, vol. 194, 164 pp., America Mathematical Society.

Page, R. (1968), Aftershocks and microaftershocks of the great Alaska earthquake of 1964, *Bulletin of the Seismological Society of America*, *58*(3), 1131–1168.

Scholz, C. (1968), The frequency-magnitude relation of microfracturing in rock and its relation to earthquakes, *Bulletin of the Seismological Society of America*, *58*(1), 399–415.

Schorlemmer, D., S. Wiemer, and M. Wyss (2005), Variations in earthquake-size distribution across different stress regimes, *Nature*, *437*, 539–542, doi:10.1038/nature04094.

Shannon, C. E. (1948), A mathematical theory of communication. Part 2, *Bell System Technical Journal*, *27*, 623–656.

Somerville, P., et al. (1999), Characterizing crustal earthquake slip models for the prediction of strong ground motion, *Seismological Research Letters*, *70*(1), 59–80.

Tata, M. N. (1969), On outstanding values in a sequence of random variables, *Probability Theory and RTelated Fields*, *12*(1), 9–20, doi:10.1007/BF00538520.

Van Aalsburg, J., W. I. Newman, D. L. Turcotte, and J. B. Rundle (2010), Record-breaking earthquakes, *Bulletin of the Seismological Society of America*, *100*(4), 1800–1805.

van Aswegen, G., and A. G. Butler (1993), Applications of quantitative seismology in South African gold mines, in *Proceedings 3rd International Symposium on Rockbursts and Seismicity in Mines, Kingston, Ontario, Canada*, edited by R. P. Young, pp. 261–266, Balkema, Rotterdam, iSBN 90 5410320 5.

van Aswegen, G., and A. J. Mendecki (1999), Mine layout, geological features and seismic hazard, *Final report gap 303*, Safety in Mines Research Advisory Committee, South Africa.

Vieira, F. M. C. C., D. H. Diering, and R. J. Durrheim (2001), Methods to mine the ultra-deep tabular gold-bearing reefs of the Witwatersrand Basin, South Africa, in *Underground Mining Methods: Engineering Fundamentals and International Case Studies*, edited by W. A. Hustrulid and R. L. Bullock, Society for Mining, Metallurgy and Exploration Inc.

Wesnousky, S. G. (1994), The Gutenberg-Richter or characteristic earthquake distribution, which is it?, *Bulletin of the Seismological Society of America*, *84*(6), 1940–1959.

Wesnousky, S. G., C. H. Scholz, K. Shimazaki, and T. Matsuda (1983), Earthquake frequency distribution and the mechanics of faulting, *Journal of Geophysical Research*, *88*(B11), 9331–9340.

Wiemer, S., and M. Wyss (2002), Mapping spatial variability of the frequency-magnitude distribution of earthquakes, in *Advances in Geophysics*, vol. 45, edited by R. Dmowska and B. Saltzman, pp. 259–302, Elsevier.

Wyss, M., C. G. Sammis, R. M. Nadeau, and S. Wiemer (2004), Fractal dimension and b-value on creeping and locked patches of the San Andreas fault near Parkfield, California, *Bulletin of the Seismological Society of America*, *94*(2), 410–421.